Improving Aviation Safety using Low-Cost Low-Fidelity Sensors Augmented with Extended Kalman Filters to Develop an Accurate Sense-and-Track System

Rohan Deshpande

Aug. 3, 2017,
revised Sept. 4, 2017,
revised Nov. 11, 2017

Abstract

In recent years, congestion in the global airspace has been increasing at an exponential rate, increasing the probability of an air collision. In addition, many companies plan to deploy autonomous aerial vehicles (drones) for commercial use in the near future, which will exacerbate congestion at low altitudes. Currently, transponder based collision avoidance systems are in use on large commercial and military aircraft, but not on smaller aircraft due to their prohibitive cost. These transponder-based systems can fail when other aerial vehicles do not have compatible transponder systems installed. Thus, it is essential that all aerial vehicles, whether they are large commercial aircraft, small private aircraft, or autonomous drones, are equipped with appropriate Collision Avoidance Systems.

I developed a low cost sense-and-track system for aerial vehicles that does not rely on a transponder based collision avoidance systems. The innovation in my method lies in replacing expensive high fidelity sensors with lower quality sensors that utilize more complex filters to develop an accurate sense and track system. My sense-and-track system consists of three components: 1) memory efficient cluster identification algorithms to identify nearby aircraft, 2) state estimation equations using Euler approximations to develop track associations to differentiate between multiple nearby moving aircraft, and 3) Extended Kalman Filters for aircraft position and velocity estimation refinements for tracking. A marine radar was used to test the sense-and-track system for tracking aircraft taking off at Boston Logan airport. The sense-and-track system accurately tracked aircraft in the local airspace, demonstrating feasibility of the low-cost radar system. Modern Collision Avoidance Systems for aircraft cost about $2 million, while the developed Sense and Avoid radar system costs only $2,000. Thus, we demonstrate that the cost of aircraft collision avoidance systems can be potentially reduced by a factor of 1000. If implemented in all aerial vehicles, this low-cost sense-and-track system can significantly improve aviation safety.

1 Introduction

In recent years, congestion in the global airspace has been increasing at an exponential rate, mirroring an increase in demand for airline flights (Fig. 1). During daily peak operations, as many as 8,000 aircraft may be operating simultaneously in the U.S. airspace [1]. To reduce the chaos in air, the Air Traffic Control (ATC) is tasked with guiding airplanes safely through the skies. With this many aircraft in flight at once, congestion and resulting flight delays are inevitable. Furthermore, many companies hope to use networks of small unmanned drones for numerous commercial applications in the near future. This will further increase congestion in the airspace, specifically at lower altitudes where aircraft are also taking-off and landing. Just recently, on October 17th 2017, a private drone crashed into a Skyjet commercial airplane in Canada, striking one of the airplane's wings [2].

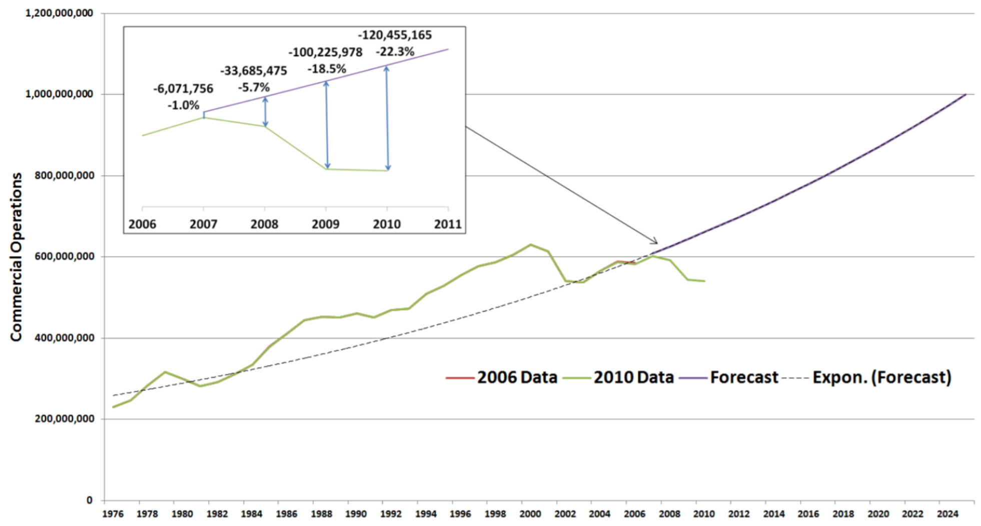

Figure 1: Airline Commercial Operations Forecast [3]

One of the current solutions to mediate air traffic congestion is to allow multiple planes to fly over each other when their trajectories intersect. Depending on the altitude difference between the two (or more) aircraft when they cross paths, this behavior can be quite risky. As the altitude difference decreases, there is less margin for error, which could be caused by pilot error or inaccurate altitude measurements. In the event that there are multiple aircraft trajectories set to intersect due to improper altitude control, an on board collision avoidance system is essential. However, the high cost of collision avoidance systems is deterrence for installing these essential Sense and Avoid Systems on smaller private aircraft or drones. This causes these smaller aircraft or drones to act as "ghosts" – undetectable to many collision avoidance systems because the systems rely on both aircraft having the correct transponders installed. There are many benefits to using radar systems to detect other flying objects, instead of transponders. One such benefit is that radar can easily detect other types of projectiles which appear in the airplane's airspace. This property is extremely useful for larger aircraft, as the radar system will allow them to detect smaller ghost aircraft. The radar system can also benefit the ghost aircraft: the cost reduction would motivate smaller aircraft or drones to install the low cost radar system if they do not already have modern sense and avoid systems installed. Thus, there is a need for a low cost, radar-based collision avoidance system for aircraft which does not rely on transponders.

My inspiration for research on cost reduction of sense and avoid systems on aircraft emerges from the automobile industry. Over the last decade, the concept of autonomous cars has gone from a prototype phase to a commercially viable product; companies, including Tesla Inc. and Google Inc., have demonstrated functional prototypes of cars driving autonomously on highways. In its current form, Tesla has successfully packaged its autonomous car software onto its current cars, labeling the software as a"Driver Assistance System." Similar to Tesla's driver assistance system, the aviation industry has also built systems to assist pilots during the flight, once the aircraft has reached its cruising altitude.

The giant leap that Google made, from demonstrating an expensive but functional prototype to actually releasing the Google-Waymo driverless car, was accomplished through numerous cost cutting strategies; in other words, the cost of the technology had to be reduced for the product to be considered as commercially viable. For example, the Google Driver-less Car used a Light Detection and Ranging (LIDAR) system to generate a 3D map of the car's surroundings. The LIDAR system utilized on their initial prototype cost $\$75,000$ [4]. One of Google's strategies was to replace the expensive and bulky LIDAR system with less expensive optical imaging technologies.

Similarly, Google's effective cost reduction strategy can also be applied to the aviation industry. Rather than using numerous astronomically expensive sensor devices, the cost can be reduced by applying modern marine radar systems to aircraft. To combat the reduction in the accuracy of the input data (due to the cheaper sensors), the input data can be filtered by exploiting the statistics of the data set in real-time.

Modern commercial aircraft use multiple sensors for Sense and Avoid systems as they are critical in mid-air aircraft collision avoidance. Currently large commercial aircraft have a Traffic Alert & Collision Avoidance System (TCAS), which includes transponders that constantly sends "pings." The pings, which operate under the radio wave frequency spectrum, allows aircraft in the vicinity to be notified of incoming air traffic and its approximate locations. Using the "pings" and approximate locations, both aircraft are able to make corrective vertical/horizontal maneuver assigned to both planes to avoid a collision. New regulations mandate that large aircraft must also have an Automatic Dependent Surveillance Broadcast system (ADS-B) installed by 2020. This newer technology involves broadcasting the aircrafts position, speed, heading, and other critical parameters [5]. When combined with the modern weather radar, the cost of these three critical technologies installed on most large aircraft is approximately \$2 million [6]. The significant cost of the Sense and Avoid Systems serve as motivation for a novel cost reduction strategy that does not compromise aviation safety.

The application of Sense and Avoid object detection systems is not limited to commercial passenger and military aircraft – they are also commonly used systems on modern Unmanned Aerial Vehicles (UAVs)[7]. With companies such as Amazon, Facebook, and Google proposing the use of a large network of UAVs, it is essential that these UAVs are equipped with the collision avoidance systems as they have to share airspace with airplanes. New UAV regulations have proposed a radar view of 220° horizontal by 40° vertical; the rational behind this new regulation is that the pilots, or in this case the computer systems on the drone must have the same field of view as real pilots on commercial aircraft [8]. The integration of radar systems and transponders on aerial systems are, as previously mentioned, astronomically expensive relative to the cost of the aircraft itself, especially for UAVs. The disregard for these systems on smaller aircraft and UAVs sharing the airspace could prove lethal, since the absence of a transponder ping would cause the aircraft to go undetected.

The limitations of the current technologies lead us to the following research questions:

- Can we develop a sense and avoid system that does not rely on other aerial vehicles having transponders?
- Can we develop low cost sense and avoid systems for aviation by using cost cutting strategies from the autonomous car industry?
- More specifically, can we replace expensive high fidelity sensors with lower quality sensors that utilize more complex filters to develop a sense and track system that can be deployed on any aerial vehicle?

2 Methods

2.1 Design Criteria

The United States Federal Aviation Administration has proposed a series of regulations dictating the conditions under which drones and UAVs flying above 10,000 feet can operate [9]. The administration proposed a minimum *view* distance of 6.4 nautical miles or 12 km. Furthermore, the UAV must have a Field Of View (FOV) of 220° horizontally around the UAV. The sensing system must also have a 40° vertical FOV. Currently, the Traffic Collision and Avoidance Systems, widely used on aircraft, operate accurately at a range of 20 NM; however, the avoidance system only issues Traffic Advisory (TA) when the two airplanes are 3.3 NM away from each other. At this distance, the pilots have 40 seconds before the impending collision, which is sufficient time for pilots to make an avoidance maneuver. The Resolution Action (RA), which demands pilots to take immediate action, is issued when the two aircraft are 2.1 NM away from each other (25 seconds before the collision). The ranges for the TCAS system are illustrated in Figure 2.

One of the main drawbacks of the TCAS system, as previously discussed, is the high cost of the system. Due to this high barrier to entry, generally only large aircraft carry TCAS systems. This leads to the other significant drawback of the system: it requires both parties to have TCAS installed. Aircraft that choose not to install TCAS due to its high cost act as “ghosts” and are

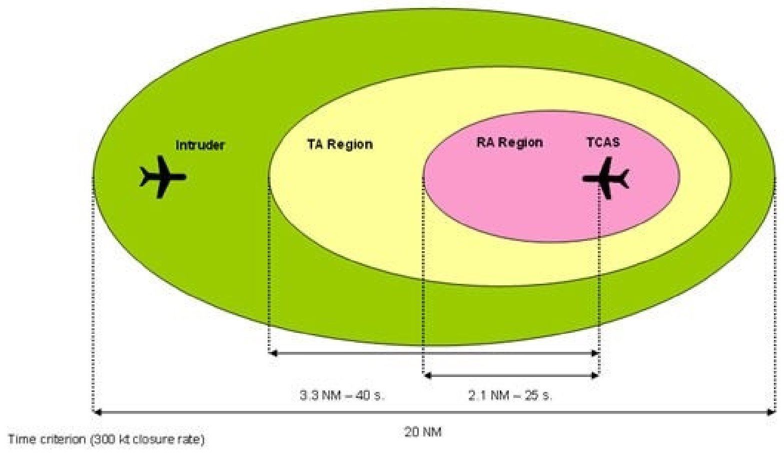

Figure 2: Ranges of TCAS

undetectable. The goal of the current research is to develop a low cost collision avoidance system that does not rely on transponders for airplane detection while still adhering to the mentioned regulations.

We decided to develop this new Sense & Avoid system by using the Simrad 4G Radar system. The radar system was chosen because it has a max range of 48 km (≈ 26 NM), which is comparable to max range of TCAS systems. This 26 NM max range would allow the radar system to be deployed in both UAV and Aircraft applications. Furthermore, the Simrad Radar costs only $\$2,000$, magnitudes less than the previously described cost of TCAS and ADS-B systems. The radar system is also low power (20 W), an essential criteria for UAVs specifically. The radar passes the criteria for Field of View (FOV) as the emitter/receiver system rotates through a full $360°$ horizontally with a $25 \pm 20\%$ vertical beam width (Fig. 3). The large vertical beam width combined with the long range of detection, allow the radar to scan a large volume of airspace for projectiles. Finally, the spinning element of the mechanical radar rotates at 48 rpm. In other words, the radar sweeps through 1 revolution every 1.25 seconds [10].

2.2 Raw Data Extraction: Radar-Computer Communication

To view the data collected from the Simrad radar, a communications system must be established between the radar and a computer. The Simrad company sells a "black box" system which acts as an intermediary device. However, this device automatically process the RAW radar data using Mini-Automatic Radar Plotting Aid (MARPA) protocols to track objects. Thus, the data sent to the computer is the tracked altered data, not the RAW radar data. This is an issue because the tracking algorithms built into the "black box" were specifically designed for tracking boats, as the radar was built for marine radar applications. The tracking abilities when tracking airplanes are woefully inadequate due to the differences in size and range of objects in marine and aviation applications. Hence I developed a host of algorithms to increase the accuracy of the radar tracking

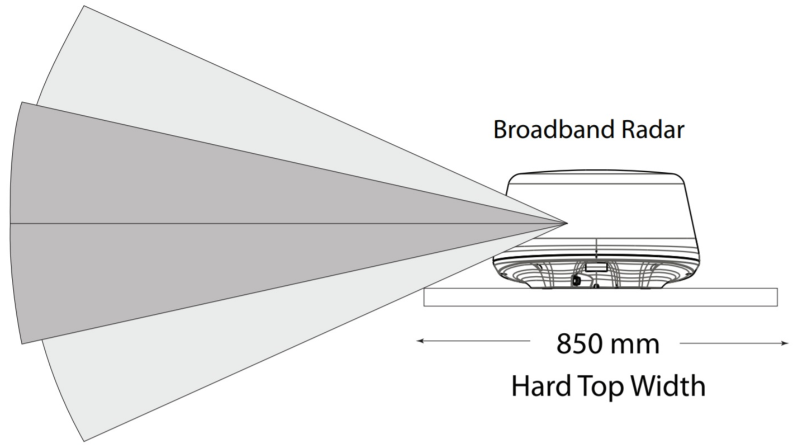

Figure 3: Vertical Angle of Radar

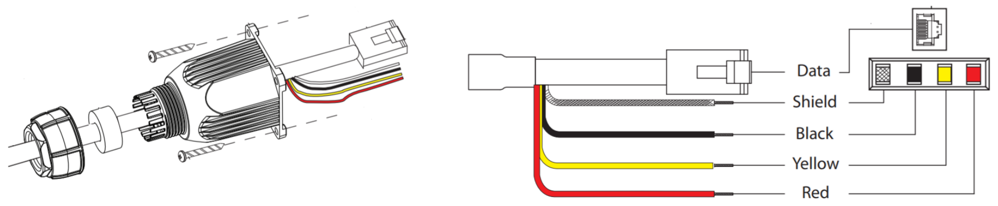

Figure 4: Radar - Computer Connections

in the aviation application. Instead of using the “black box” extension, I connected the radar to a computer by reverse engineering the communications protocol. The numerous wires protruding from the radar were split into two categories: power connections and data connections. The four power connections include two 24V lines (red and yellow) and a ground line (black). The data connections include 8 wires, which are mapped to the pins of an Ethernet cable. When plugged directly into a computer or through an Ethernet switch, the radar is assigned an IP address on which it will communicate with the computer. To retrieve data from the radar over the Ethernet, I wrote multiple C++ scripts. The radar defaults to low power mode when it is first connected to the 24V power supply. The radar waits for a specific *wake up* command to be sent over the ethernet port to actually turn the radar on. I found this data signal through reverse engineering the Simrad proprietary communications device. Once the radar system accepts this signal, it automatically sends RAW data; however, one of the issues with the data transmission is that the data is not sent at a constant rate. To solve this issue, a Watchdog Timer is set after the end of each radar transmission. If the computer does not receive the next transmission before the timer expires, the code throws an error. Otherwise, the radar/computer interface functions as expected.

Three separate parameters are passed to the C++ code, which receives the data in binary from the radar: radius, angle, and return strength. These values, represented as a combination of bytes, are converted to the standard integer values with the correct bounds that C++ expects. At each discrete raw angle, as the radar revolves, a new vector of data is sent to the C++ script. The indices of the vector represent the radii while the values represent the strength return. Each new vector being transmitted will be referred to as a “spoke”, since it refers to a “slice” of data from a full circle. The radius ranges from 0 to 511, angle ranges from 0 to 2047, and the return strength ranges from 0 to 255. The data can be graphed in realtime using a C++ script which converts the polar coordinate values (raw radius and raw angle) and transforming it into Cartesian coordinates. To visualize the third dimension (strength return of the radar signal), the colors of the pixels are varied between black (no return), blue (low return), and red (high return). The computer’s mouse scroll wheel control was mapped to the `changeRange()` function. The function transmits a series of binary values that command the radar to change its max range. The max ranges are fixed by the manufacturers of the radar and range between 50 m and 48 km. Note that the number of radius values returned remains constant (512) regardless of the max range since the raw radius is relative. Each individual data value, which is a combination of radius r, angle θ, and strength s, will be referred to as a pixel p. The difference in resolution of the pixel at different ranges is illustrated:

$$p = \{r, \theta, s\}$$

The resolution of the radius is defined as the number of pixels per meter:

$$R = \frac{512}{r_{max}}$$

If the max radius is 50m, the resolution is 10.2 pixels/m; however, if the max range is set to 48km, the resolution reduces to 0.01 pixels/m. The typical wingspan of a commercial aircraft is 30 m. By rearranging the equation for resolution, it is evident that the max range of the radar should be set to values less than $\approx$ 16 km for aircraft to appear larger than 1 pixel.

2.3 Radar Calibration

To make sure the reverse engineered communications protocol was working accurately, I installed the radar system on the roof of the Aurora Science Building so that the radar system had a full view of the Boston-Cambridge skyline. The data as the radar sweeps through 360° was superimposed on top of the geographic map of the Cambridge/MIT area to gain a physical meaning from the data. High radar returns, shown in red, are concentrated over the Harvard Bridge and the skyscrapers in Boston. Thus, the superimposed map shows consistency between the radar data and the physical world.The accuracy of the radar system was determined by measuring the length of multiple objects in the radar field of view, such as the Harvard Bridge, and comparing these values with their actual lengths. The percent error of all these measurements were found to be within 1% of the actual length of the objects. Thus, the radar was determined to be properly calibrated.

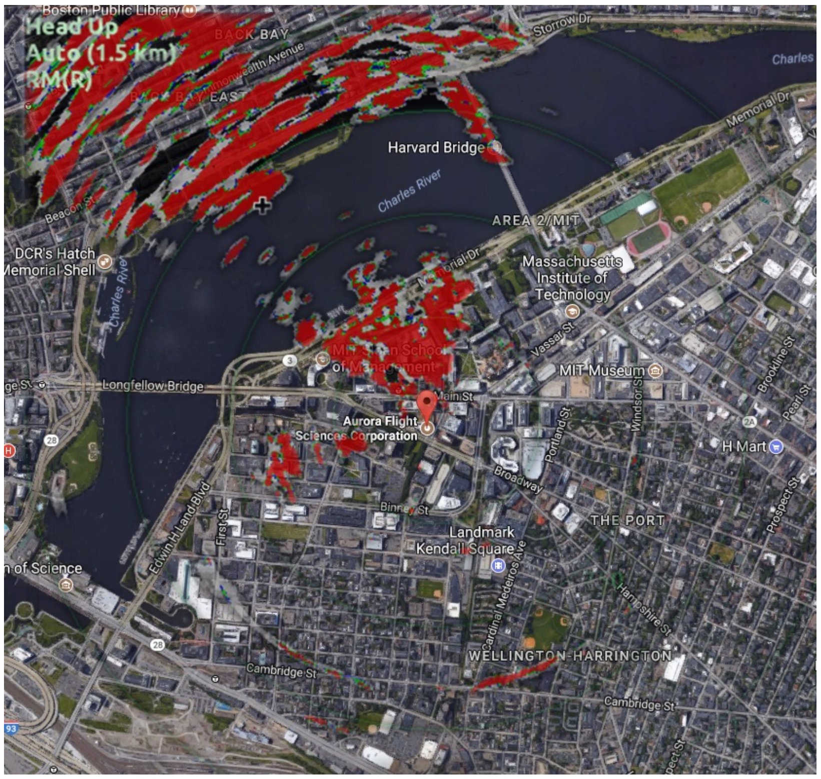

Figure 5: Map with Radar Values

2.4 Development of Memory Optimized Cluster Identification Algorithm

The calibrated radar sends a 2-D matrix of strength returns to the computer. However, this matrix must be processed to actually identify the exact locations of any airplanes that are visible in the radar's field of view. An aircraft will be visible as a group of pixels with non-zero values in the 2-D matrix. We define the word *cluster* as a grouping of pixels that all have non-zero strength returns and are adjacent to at least one other pixel in the group that represent an aircraft.

Modern cluster identification Algorithms import the full 2-D matrix before identifying the clusters. However, it is impractical to load the whole raw data set and then run traditional cluster recognition algorithms, because RAW data is logged into a `.txt` file at the rate of 1Gb every minute. In merely 10 minutes of data capture, the raw data set would consume 10Gb of RAM on a computer. Thus, it is essential that a memory optimized cluster identification algorithm is developed to overcome the shortcomings of the application of traditional cluster recognition algorithms in big data applications. Traditional cluster identification programs also cannot be used because they rely on the fact that all the data is taken at the same time (e.g. camera). The radar, however, transmits data one spoke at a time, meaning that the data at angle 2047 was taken ≈ 1.25 seconds before the data at angle 0.

I developed a memory optimized cluster identification algorithm that works by only storing the last two columns of the data set (current and previous spoke). When these two columns are processed, a new spoke from the radar is appended to the 2-D matrix. The new last two columns

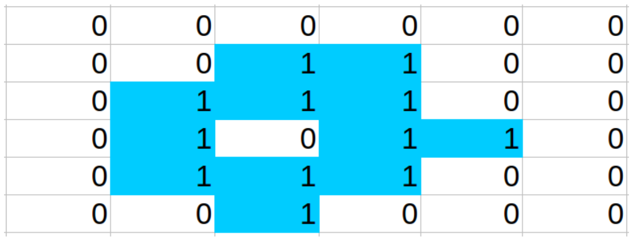

0	0	0	0	0	0
0	0	1	1	0	0
0	1	1	1	0	0
0	1	0	1	1	0
0	1	1	1	0	0
0	0	1	0	0	0

Figure 6: Data of Cluster Identification Algorithm

in the data set (the new current and previous spoke) are processed. Thus, at any given time the computer is only storing two columns of data, reducing the amount of RAM needed to run the script to a mere 20 kB. Thus, the required memory to run the script is reduced by a factor of 50,000. To visualize the processing algorithm, observe Figure 6, which illustrates the full input data in the form of a two dimensional array. Note that the illustration simplifies the data by representing all non-zero values as 1, so that the matrix appears to be a binary *hit* or *miss*. The cluster identification algorithm (Algorithm 1) begins by looping through all the pixels in a single vertical column and identifying all adjacent non-zero pixels. Each of the concurrent strings of adjacent pixels is stored in a specialized `Cluster` class. This class holds an array of all the pixels, the minimum radius value, the maximum radius value, and the area. The minimum and the maximums of the clusters from the new spoke are compared to the min and max of the previously identified clusters from the last spoke. If the clusters overlap `if(!((min1>max2)||(min2>max1)))`, then the clusters are merged. Any clusters from the previous spoke that are not merged with new clusters have been fully combined and are excluded from the merging process at the next step. When a cluster is finished merging, the center of the cluster is calculated using the following formulas:

$$x_{cent} = \frac{\int x dA}{A}, \quad y_{cent} = \frac{\int y dA}{A},$$

This formula for the center assumes that x_{cent} is mapped to the RAW angle, and y_{cent} is mapped to the RAW radius. Using the mentioned algorithm, data collected from the radar (which was stored in a `.txt` file) was automatically post-processed. The input data is graphed as a two dimensional array with the colors representing the return strength of the radar signal (see figure 7).

Each of the 24 clusters in the data were accurately identified by the algorithm, and the centers (in terms of r and θ) were recorded.

2.5 Tracking and Predicting Clusters over Time

The cluster identification algorithm identifies and returns the position of the aircraft in the field of view at each snapshot in time. To track the aircraft, the position of the aircraft at each of the snapshots, hereafter referred to as *timestep*, must be strung together. If the cluster identification algorithm only identifies one airplane, correlating the motion of of the airplane at each time step is straightforward – each time the radar sweeps through a complete 360°, we see the aircraft's new

Algorithm 1 Cluster Identification

```
1:  while new spoke != NULL do                                  ▷ run for each new spoke from radar
2:      for current pixel in new spoke do
3:          if current pixel!=0 and previous pixel=0 then
4:              Create temp Cluster
5:              temp.low ← pixel index
6:          else if current pixel!=0 then
7:              Add pixel to temp
8:          else if current pixel = 0 & previous pixel!=0 then
9:              temp.high ← pixel index-1
10:             Push temp cluster to new clusters list       ▷ new clusters is a list of cluster objects
11:         end if
12:     end for
                  ▷ We must compare new clusters list and old clusters list and merge adjacent clusters
13:     $a, b = 0$                                    ▷ a is old clusters index, b is new clusters index
14:     for $a$ <old clusters size & $b$ < new clusters size do
15:         if old clusters[a].high < new clusters[b].low then
16:             $a++$
17:         else if new clusters[b].high < old clusters[a].low then
18:             $b++$
19:         else                                                ▷ true only if clusters are adjacent
20:             Merge old cluster[a] and new cluster[b]
21:         end if
22:     end for
23:     old clusters = new clusters                                         ▷ prepare for next spoke
24: end while
```

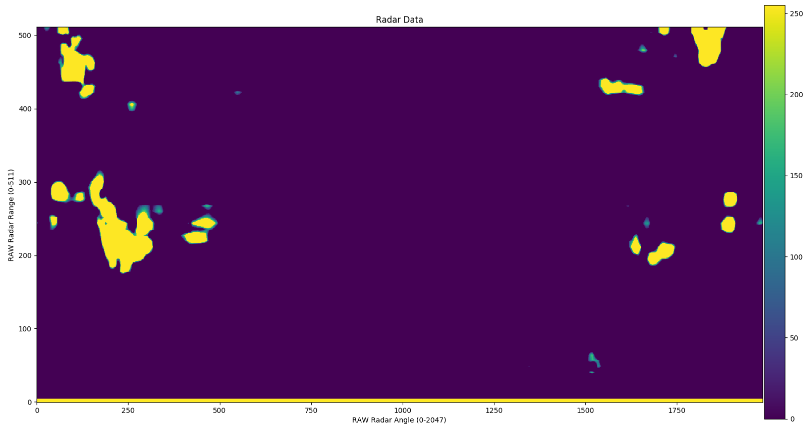

Figure 7: RAW Radar Data as 2-Dimensional Array

location. However, correlating the positions from the previous and current time steps is much more difficult when there are multiple aircraft's identified by the algorithm. In the case that two aircraft pass by each other, the previously mentioned method would fail because it wouldn't know which one of the two clusters from the previous time step correlates to the two new clusters. The accurate stringing of the locations of the airplanes at each time step is called *track association*.

As the radar system detects local aircraft with each 360° sweep, the position of the aircraft changes significantly. This phenomenon occurs due to the change in time between each sweep. For a standard commercial aircraft with a cruising speed, $v_{cruising}$ of 900 km/hr, the change in position for an aircraft at cruising speed can be estimated as follows:

$$\Delta t = \frac{1}{T} = \frac{1}{48 rev/min} \frac{60 sec}{min} = 1.25 seconds$$

$$v_{cruising} \approx 900 km/hr, \quad \Delta d = v_{cruising} \Delta t = 312.5 m$$

Thus, in a single 360° sweep, the aircraft being tracked has traveled more than 6 times its body length. Coupled with the low resolution of the radar system, the position of the aircraft seems to make sudden *jumps* between frames. The significant changes in position due to the discrete time domain is also problematic when the radar system attempts to track multiple objects; as the objects converge, it becomes increasingly difficult to determine where each individual object moved. To overcome this drawback of the lower resolution radar, I developed a state estimation algorithm to estimate the position of the aircraft at the next radar sweep. The predictions can then be compared to the actual locations of aircraft to correlate the data from the current and previous time steps.

2.5.1 Track Initializer

I wrote the Track Initializer algorithm (Algorithm 2) to examine and correlate the clusters from two different time steps to determine where each airplane moved. The algorithm begins by computing a vector addition, converting the nearby airplane's coordinates with respect to the radar to coordinates with the earth frame of reference. As a result, comparing the coordinates of the airplane at two time steps yields the true velocity (relative to the ground) of the airplane. The distance between each of the initial clusters to each of the new clusters is compared to a pre-defined normal distribution (created based on the average cruising speed of aircraft and the period of the radar sweep). Each of the z-scores less than 5 standard deviations is considered a potential candidate (military aircraft are just below 4 standard deviations) and added to a list of potential tracks. For each potential match in the list, the position at the next (third) time-step is predicted based on the Euler Approximation. If the third point prediction closely matches the actual position at the next sweep, within a predefined threshold, then the three points can be inputted into the tracking algorithm.

Position Prediction using Euler Approximations The Euler Approximation method makes a prediction by exploiting the fact that aerial vehicles travel roughly linearly– that is, there aren't rapid speed changes or direction changes on the radar's timescale. The method uses the position data at the current time step and velocity (calculated using the current and previous time steps). The position vector, between the radar and tracked aircraft, is defined by r and θ. Similarly, the two velocity vectors are represented in polar coordinates by (v_1, θ_1) and (v_2, θ_2) respectively. The subscript k represents the state during the current time step, while the subscript $k-1$ represents the state at the previous time step.

Algorithm 2 Track Initializer

```
1: for new points do
2:     $x = x_o + v_x t$                                   ▷ Change to earth frame of reference
3:     $y = y_o + v_y t$
4: end for
5: Define Normal Distribution: $N(\mu, \sigma^2)$
6: for initial points do
7:     for new points do
8:         $d = \sqrt{(\Delta x)^2 + (\Delta y)^2}$
9:         $z = (d - \mu)/\sigma$
10:        if $z < 5$ then
11:            add to potential tracks
12:        end if
13:    end for
14: end for
15: for each list of potential tracks do
16:    for each element in potential track do
17:        point3$\{\hat{x}, \hat{y}\} = \textit{predictPoint}$(point1, point2)   ▷ Predict using Euler Approximations
18:        $d_{new} = \sqrt{(x - \hat{x})^2 + (y - \hat{y})^2}$
19:        if $d_{new} <$ Uncertainty Threshold then           ▷ True when Prediction is close
20:            Start tracking using point1, point2, point3
21:        end if
22:    end for
23: end for
```

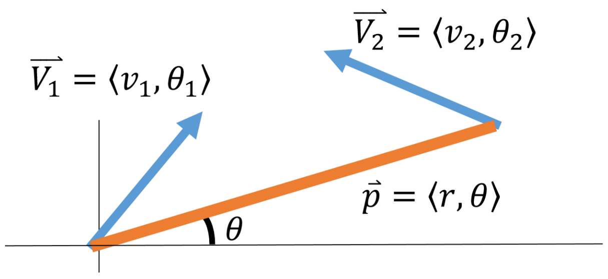
$\vec{V_1} = \langle v_1, \theta_1 \rangle$
$\vec{V_2} = \langle v_2, \theta_2 \rangle$
$\vec{p} = \langle r, \theta \rangle$
θ

Figure 8: Motion of Two Aircraft in Polar Coordinates

The radius at the next sweep is estimated based on previous known parameters:

$$r = \sqrt{x^2 + y^2}$$

$$\frac{\partial r}{\partial t} = \frac{1}{2}(x^2+y^2)^{-1/2} * \left(2x\frac{\partial x}{\partial t} + 2y\frac{\partial y}{\partial t}\right)$$

$$\frac{\partial x}{\partial t} = v_x = v_1\cos\theta_1 + v_2\cos\theta_2$$

$$\frac{\partial y}{\partial t} = v_y = v_1\sin\theta_1 + v_2\sin\theta_2$$

To calculate $\dot{r}$, I next converted from Cartesian to polar and substituted the velocities v_x and v_y.

$$\dot{r} = \begin{bmatrix}\cos\theta & \sin\theta\end{bmatrix} \cdot \begin{bmatrix} v_1\cos\theta_1 + v_2\cos\theta_2 \\ v_1\sin\theta_1 + v_2\sin\theta_2 \end{bmatrix}$$

$$\hat{r}_k = \hat{r}_{k-1} + \Delta t \begin{bmatrix}\cos\theta_{k-1} & \sin\theta_{k-1}\end{bmatrix} \cdot \begin{bmatrix} v_{1k-1}\cos\theta_{1k-1} + v_{2k-1}\cos\theta_{2k-1} \\ v_{1k-1}\sin\theta_{1k-1} + v_{2k-1}\sin\theta_{2k-1} \end{bmatrix}$$

The angle after the next sweep is also estimated based on the previous known parameters:

$$\theta = \tan^{-1}(y/x)$$

$$\dot{\theta} = \frac{1}{1+y^2/x^2}\left(\frac{1}{x}\frac{\partial y}{\partial t} - yx^{-2}\frac{\partial x}{\partial t}\right)$$

$$\dot{\theta} = \frac{1}{x^2+y^2}\left(-y\frac{\partial x}{\partial t} + x\frac{\partial y}{\partial t}\right)$$

To calculate $\dot{\theta}$, I next converted from Cartesian to polar and substituted the velocities v_x and v_y.

$$\dot{\theta} = \begin{bmatrix}-\sin\theta/r & \cos\theta/r\end{bmatrix} \cdot \begin{bmatrix} v_1\cos\theta_1 + v_2\cos\theta_2 \\ v_1\sin\theta_1 + v_2\sin\theta_2 \end{bmatrix}$$

$$\begin{bmatrix}-\sin\theta_{k-1}/r_{k-1} & \cos\theta_{k-1}/r_{k-1}\end{bmatrix} \cdot \begin{bmatrix} v_{1k-1}\cos\theta_{1k-1} + v_{2k-1}\cos\theta_{2k-1} \\ v_{1k-1}\sin\theta_{1k-1} + v_{2k-1}\sin\theta_{2k-1} \end{bmatrix}$$

$$\hat{\theta}_k = \hat{\theta}_{k-1} + \Delta t\dot{\theta}_{k-1}$$

2.5.2 Track Association using an Extended Kalman Filter

Technically, it is possible to continuously track the aircraft using the Euler Approximation method. However, this method is only accurate when aircraft are not changing directions of speeds. This acts as a significant drawback when two aircraft approach each other because the crude approximation could accidentally lock onto the wrong aircraft – switching the tracks. The proposed tracking method uses a Kalman Filter to create a more accurate prediction of the location of the aircraft. The refined prediction is created due to the iterative process of the Kalman Filter, which drives the error in prediction to zero. Thus, the track initialize determines three points from the same aircraft and inputs these points into the Kalman Filter, which tracks the aircraft in real-time.

The implementation of the Kalman filter first transforms the data from the radar, which is represented in a r and θ polar coordinate system, to Cartesian coordinates. However, due to the nonlinear nature of the transformation, a standard Kalman Filter cannot be used. Instead, an Extended Kalman Filter (EKF) is implemented, which linearizes about an estimate of the current mean and covariance in the discrete time domain.

Polar to Cartesian Conversion for State Matrix

$$\begin{bmatrix} \theta \\ r \end{bmatrix} \longrightarrow \begin{bmatrix} r_k \cos\theta_k \\ r_k \sin\theta_k \\ (r_k \cos\theta_{k-1} - r_{k-1}\cos\theta_{k-1})/\Delta t \\ (r_k \sin\theta_{k-1} - r_{k-1}\sin\theta_{k-1})/\Delta t \end{bmatrix} = \begin{bmatrix} x \\ y \\ \dot{x} \\ \dot{y} \end{bmatrix} = \hat{X}_k$$

Predicting the State Matrix The prediction of $\hat{X}$ at the new state is approximated through linearization.

$$\hat{X}_k = A * \hat{X}_{k-1}$$

$$\hat{X}_k = \begin{bmatrix} 1 & 0 & \Delta t & 0 \\ 0 & 1 & 0 & \Delta t \\ 0 & 0 & 1 & 0 \\ 0 & 0 & 0 & 1 \end{bmatrix} * \hat{X}_{k-1}$$

The correlation between the position and velocity components of $\hat{X}$ are captured in the covariance matrix P. Each element in the matrix, P_{ij}, represents the degree of correlation between the *ith* state variable and the *jth* state variable. The covariance matrix is predicted as follows:

$$P_{k|k-1} = AP_{k-1}A^T + WQ_{k-1}W^T$$

Updating the State Matrix Based on the predicted state matrix and covariance matrix, the Kalman gain K is calculated:

$$K = \frac{P_{k|k-1}H_k}{H_k P_{k|k-1} H_k^T + R}$$

Intuitively, the Kalman gain acts as a correction factor used during the prediction phase of each iteration. The Kalman gain is updated in order to drive the residual of the predicted and observed states to zero. The observational model matrix H_k is defined as the Jacobian of the inputted data.

$$H_k = \frac{\partial h}{\partial x}|_{\hat{x}_{k|k-1}}$$

Since the inputted data is in terms of θ and r, the observational model is found to be:

$$h = \begin{bmatrix} \theta \\ r \end{bmatrix} = \begin{bmatrix} \tan^{-1}(y/x) \\ \sqrt{x^2 + y^2} \end{bmatrix}$$

$$H = \begin{bmatrix} \partial\theta/\partial x & \partial\theta/\partial y \\ \partial r/\partial x & \partial r/\partial y \end{bmatrix} = \begin{bmatrix} \frac{-y}{x^2+y^2} & \frac{x}{x^2+y^2} \\ \frac{x}{\sqrt{x^2+y^2}} & \frac{y}{\sqrt{x^2+y^2}} \end{bmatrix}$$

The states are updated based on both previous predictions and new data regarding the current state. An essential step to this calculations involves determining the residual between the predicted state $\hat{X}_k$ and the actual state z_k. The data input at the current state k is written as:

$$z_k = h(\hat{X}_k) + v_k$$

The measurement of residual is defined as $\hat{y}_k = z_k - h(\hat{X}_{k|k-1})$ This residual and Kalman gain are directly related to the change in the values of the state matrix during the update process.

$$\hat{X}_k = \hat{X}_{k-1} + K\hat{y}_k$$

On the other hand, the covariance matrix is updated by considering the Kalman gain and the observational model.

$$P_{k|k} = (I - KH)P_{k|k-1}$$

The prediction and update processes are iterated through at each time step in the discrete time domain. In other words, at the end of each loop $\hat{X}_k$ becomes $\hat{X}_{k-1}$ and $\hat{P}_k$ becomes $\hat{P}_{k-1}$ based on the properties of recursion. The updated states, which are now considered to originate from state $k-1$ instead of k, now form the input matrix of our next prediction. The outlined Extended Kalman Filter was integrated into the C++ code for the tracking algorithm.

2.5.3 Sense and Track Method

I developed a memory efficient cluster identification system, track initializer algorithm, and accurate Extended Kalman Filter tracking system. Finally, I outline a unifying algorithm which utilizes each of the mentioned algorithms to create a full Sense and Track method. At each sweep the cluster identification algorithm creates a list of clusters found at the current time. The clusters fall in three categories: clusters that were already being tracked, clusters that were untracked but had predictions, and clusters that were untracked and did not have predictions. The algorithm begins by matching clusters that were already being tracked to clusters at the current time step (using the EKF predictions made at $t-1$). Similarly, clusters that were untracked but had Euler Predictions from $t-1$ are matched with the remaining clusters at the current time step. Once a 1-1 match is found, the position data at the two time steps is inputted to the EKF to begin the accurate tracking procedure. The remaining elements in current clusters list are untracked clusters without predictions, since the matched clusters are removed from the list. The remaining clusters (from t) and the untracked clusters without predictions (from $t-1$) are inputted to the tracking initializer algorithm, which is outlined in section 2.5.1. The track initializer process finds all potential matches between the untracked clusters at t and $t-1$ and makes predictions for the position at $t+1$. Once the predictions are made, these clusters will move up to the "untracked clusters with predictions"

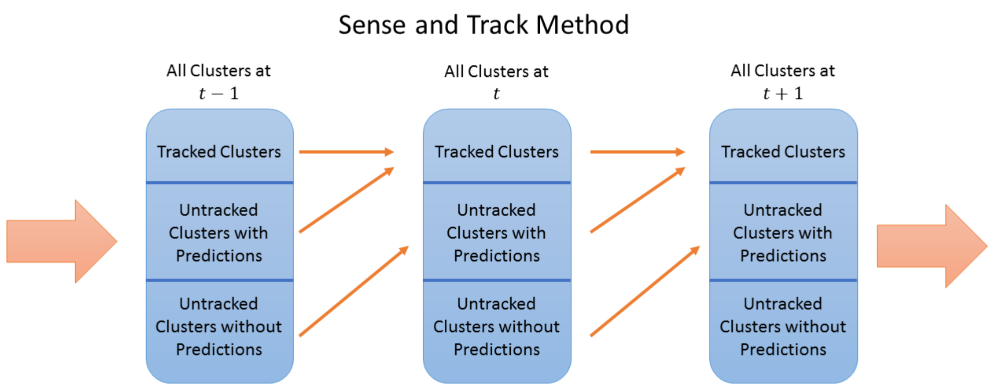

category for the next time step. Thus, within three time steps a new cluster can be tracked with an EKF.

Algorithm 3 Sense and Track Algorithm

```
 1: $T$ ←Tracked Clusters with predictions            ▷ prediction made using data at $t-1$
 2: $P$ ←Untracked Clusters with predictions          ▷ prediction made using data at $t-1$
 3: $U$ ←Untracked Clusters without predictions       ▷ cluster data from state $t-1$
 4: $C$ ←Current Clusters                              ▷ data from state $t$
 5: for $T' \in T$ do
 6:     Find closest match: $T' \approx C' \in C$
 7:     Remove $C'$ from $C$
 8:     Continue EKF Tracking with $C'$
 9: end for
10: for $P' \in P$ do
11:     Find closest match: $P' \approx C' \in C$
12:     Remove $C'$ from $C$
13:     Begin EKF Tracking with the two points
14: end for
15: Tracking Initializer ($U$, $C$)   ▷ Finds all potential matches between untracked clusters at $t$ and
    $t-1$. The track initializer also makes a prediction for the position at $t+1$ (see section 2.5.1)
```

2.6 Collection of Truth Data using ADS-B

To determine the accuracy of the radar system, the output data from the Extended Kalman Filter must be compared to some form of *truth data* which includes the actual position and velocity at a given time. This *truth data* is collected using Automatic Dependent Surveillance - Broadcast (ADS-B). The ADS-B technology works by broadcasting information about an aircraft's GPS location, altitude, ground speed and other data to ground stations and other aircraft, approximately once per second. Air traffic controllers and aircraft equipped with ADS-B can immediately receive this broadcasted information [11].

I installed a low cost ADS-B monitoring system operating at 978 MHz at the Aurora Flight Sciences building and used to record the broadcasted data from nearby aircraft as they begin their ascend after taking-off from Boston-Logan International Airport. I wrote multiple scripts in C to handle the ADS-B to USB to computer communications, parse the proprietary data communication protocol, log relevant data to `.txt` files, and graph the positions of the aircraft in real-time on top of a Google map using the Google Maps API.

After the ADS-B is parsed, it must be converted into the same matrix system as the radar. The ADS-B data is originally in the form of Latitude-Longitude-Altitude (LLA); however, the radar data is logged in a North East Down (NED) format. To convert between LLA to NED, an intermediary conversion must occur. Initially the Earth-centered Earth-fixed (ECEF) position is calculated from geodetic latitude, longitude, and altitude (LLA) above planetary ellipsoid. The formula for this conversion is as follows [12]:

$$\vec{p} = \begin{bmatrix} p_x \\ p_y \\ p_z \end{bmatrix} = \begin{bmatrix} r_s \cos\lambda_s \cos t + h\cos\mu\cos t \\ r_s \cos\lambda_s \sin t + h\cos\mu\sin t \\ r_s \sin\lambda_s + h\sin\mu \end{bmatrix}$$

where the geodetic latitude ($\bar{\mu}$), longitude ($\bar{\imath}$), and altitude ($\bar{h}$) above the planetary ellipsoid into a 3-by-1 vector of ECEF position ($\bar{p}$). The geocentric latitude at mean sea-level and the radius at a surface point (r_s) are defined by flattening ($\bar{f}$), and equatorial radius ($\bar{R}$) in the following relationships:

$$\lambda_s = \arctan((1-f)^2 \tan\mu)$$

$$r_s = \sqrt{\frac{R^2}{1 + (1/(1-f)^2 - 1)\sin^2\lambda_s}}$$

The intermediate ECEF format is converted into the desired NED format using the following formula [13]:

$$DCM_{ef} = \begin{bmatrix} -\sin\mu\cos t & -\sin\mu\sin t & cos\mu \\ -\sin t & \cos t & 0 \\ -\cos\mu\cos t & -\cos\mu\sin t & -\sin\mu \end{bmatrix}$$

such that DCM_{ef} represents the Direction Cosine Matrix, which captures the rotation about the longitudinal axies and latitudinal axes.

3 Low Cost Radar System Testing and Results

3.1 Testing of Radar Tracking Algorithm

I tested the State Estimation Algorithm with the Extended Kalman Filter by tracking aircraft in the local airspace near the Boston-Logan International airport. The Simrad 4G radar system was installed on top of the Aurora Flight Sciences Research and Development Office in Cambridge, Massachusetts. The building is located ≈ 6 km from the airport. The radar's ability to track the

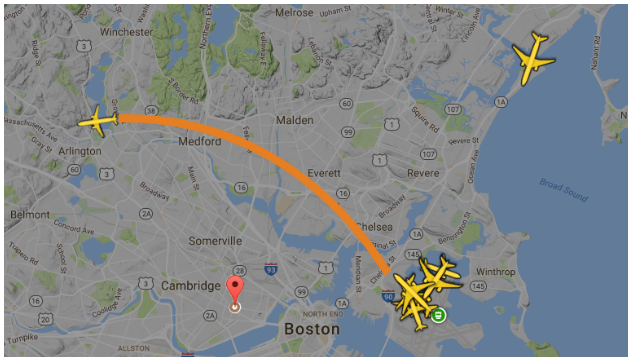

Figure 9: Take-Off Flight Plan from Boston-Logan Airport

airplanes were determined by multiple non-controllable factors:

- Weather Conditions – the radar cannot be operated outdoors during the rain as it is not properly electrically insulated currently. The solution to this issue is to apply heat-shrink tubing to the solder joints such that the metal is not exposed, allowing it to be water proof. The entry points for all cables externally connected to the radar system (including the power connection and multiple data connections) should be sealed with water-proof rubber connectors.
- Wind Direction – Air Traffic Control (ATC) generally directs airplanes to take-off and land while moving into the wing (so that they do not have any tail wind). The Aurora Flight Sciences Building is located due west of the airport; thus, aircraft cannot be tracked if they approach the airport in the east -west direction. Similarly, if aircraft are forced to take-off in the west to east direction, they will not be able to be tracked as the flight path will never pass by the building.

Although these factors seem to be significant limitations to the Low Cost Radar System technology, they only apply to the case where the radar has a zero velocity near the airport. When installed on an airplane, the weather conditions and wind direction will have no impact on the track itself; these parameters only changed the aircraft's preferred route during ascension or descension.

Radar data was collected on July 28th, 2017. Due to the south-east facing wind direction, during the data collection time frame the wind direction pointed North West facing runway for take-off. As airplane took-off, they curved leftwards in a large circular fashion around the Cambridge city area.

The data from the radar was once again unwrapped to form an image for each revolution of the radar angle sweep. It was hypothesized that only a few returns would pick up the airplane due to the relatively far range the radar was operating at along with the radar's low resolution. As demonstrated in Figure 10, the airplane is hardly visible when viewing the whole image. In fact, out of the $\approx 1,000,000$ returns in each revolution's matrix (512×2048), only 5 returns were from the actual airplane. The 2-D matrix at each time step was subtracted from the previous time step to locate all the clusters that were moving. This removed all the large yellow stationary spots near

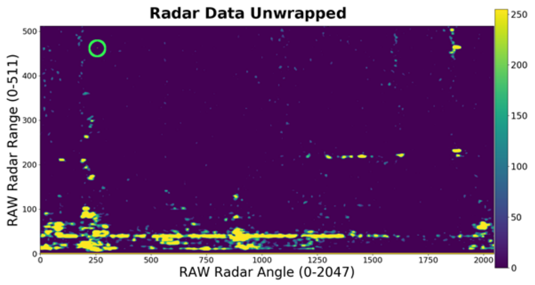

Figure 10: Unwrapped Radar Data for One Revolution – data contains Airbus A320-232 airplane being tracked

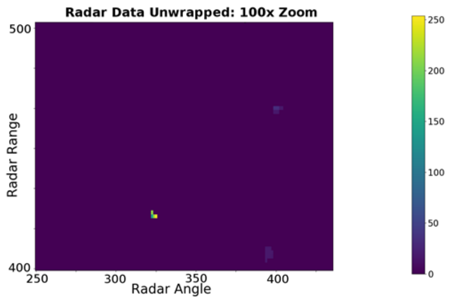

Figure 11: Magnified Image – bright yellow spot near $r \approx 325$ and $\theta \approx 425$ is the Airbus A320-232 being tracked

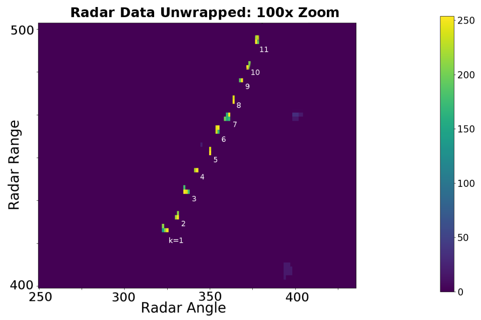

Figure 12: Magnified radar data for each time step overlayed

the bottom of the matrix which were the tops of buildings in the Boston/Cambridge skyline. In Figure 10, the airplane is the tiny yellow dot near an angle of 300 and a radius of 450. To assist the determination of the location of the airplane, a bright green circle was placed around the airplane's yellow dot, such that the yellow dot is at the center of the circle. Figure 11 shows the initial image magnified by a factor of 100.

The location of the airplane was tracked for 11 frames as the airplane passed through the field of view of the radar. Although the airplane is difficult to identify from the RAW unwrapped data, the airplane is easily distinguishable when the data is magnified by a factor of 100. Each of the images from the 11 frames were superimposed on top of each other to display the airplane's position through each of the time steps (Fig. 12). Each of the positions of the airplane is labeled on the image by the time steps ranging from $k = 1$ to $k = 11$.

3.2 Determining Accuracy of Airplane Track

The ADS-B parsing algorithm returns the ADS hex code, which acts as an aircraft's unique signature, epoch time, radius r, angle in the horizontal plane θ, and angle in the veritcal plane ϕ. Each of the spherical coordinate values is converted into the raw data format that the radar outputs. The conversions are as follows:

$$r_{RAW} = 512\frac{r}{8000}, \quad \theta_{RAW} = 2048\frac{\theta}{360}, \quad \phi_{RAW} = 2048\frac{\phi}{360}$$

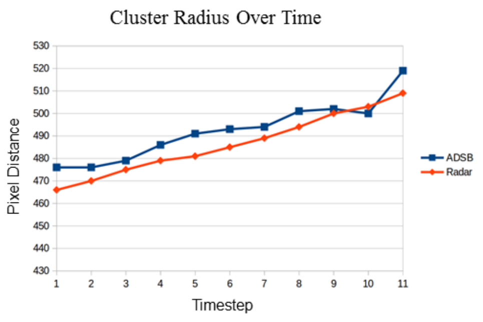

Figure 13: ADS-B Truth Data and Radar Data

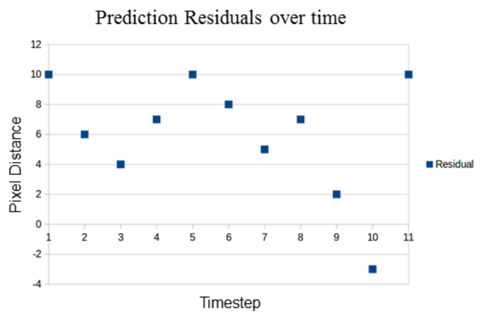

Figure 14: ADS-B v. Radar Residual Plot

Since both ADS-B data and Radar cluster position data are now using the same units, both data sets can be graphed against each other with the ADS-B data acting as the truth data. As the radar collects the strength return data, the Extended Kalman Filter algorithm sifts through all the identified clusters and noise, and outputs the exact location of the aircraft.The similarity/difference between the position data provided by the EKF and the truth data can be numerically identified by calculating the root mean squared error (RMSE). The RMSE measures the square-root of the average error squared between the EKF data and ADS-B data. We define the actual radius of the object from the ADS-B sensor as r_i and the radius value from the radar sensor as $\hat{r}_i$. The Root Mean Squared Error is calculated as follows:

$$RMSE = \sqrt{\frac{1}{n}\sum_{i=1}^{n}(\hat{r}_i - r_i)^2}$$

Using the mentioned formula for root mean squared error, the $RMSE$ was calculated to be 7.084. Theoretically, the RMSE should tend to zero when the radar measurements are accurate relative to the ADS-B data. Errors in the radar measurements could include inaccurate calibration of the 9-axis heading sensor, inaccuracies in the initial GPS coordinate of the radar system, and inaccuracies due to low radar resolution. The error is clearly visible in the residual plot, which shows the residuals being skewed to the positive end rather than being centered at zero. This means that the radar consistently underestimates the position. If the zero error was corrected, the RMSE would drop to 3.77, showing a mere 0.5% error in aircraft position measurement. Thus, the Extended Kalman Filter can provide an accurate track association of an aircraft.

4 Conclusion and Other Applications

Modern collision avoidance systems for aircraft have been historically astronomically expensive, deterring many smaller aircraft from using collision avoidance systems. Refraining from using the collision avoidance systems is dangerous for both the small ghost aircraft and the large commercial aircraft, since commercial aircraft cannot detect and avoid the smaller aircraft when they do not have transponders installed. I set a goal of developing a low cost sense-and-track system for aerial vehicles that does not rely on a transponder based collision avoidance systems.

The innovation in my method lies in replacing expensive high fidelity sensors with lower quality sensors that utilize more complex filters to develop an accurate sense and track system. My sense-and-track system consists of three components: 1) memory efficient cluster identification algorithms to identify nearby aircraft, 2) state estimation equations using Euler approximations to develop track associations to differentiate between multiple nearby moving aircraft, and 3) Extended Kalman Filters for aircraft position and velocity estimation refinements for tracking. A marine radar was used to test the sense-and-track system for tracking aircraft taking off at Boston Logan airport. Furthermore, position data from the radar system was compared to the true values from the ADS-B. The sense-and-track system accurately tracked aircraft in the local airspace showing a mere 0.5% error in aircraft position measurement, thus, demonstrating the low-cost radar-based sense-and-track system's feasibility. Modern Collision Avoidance Systems for aircraft cost about $2 million, while the developed Sense and Avoid radar system costs only $2,000. Thus, I also demonstrate that the cost of aircraft collision avoidance systems can be potentially reduced by a factor of 1000.

In the near future, big tech companies including Amazon, Google, and Facebook plan to use fleets of drones for their services. The introduction of drones into regulated airspace will further increase the congestion in the global airspace. Thus, it is essential that these drones also have collision avoidance systems, so that they can sense and avoid both drones and aircraft. It is unlikely that a standardized transponder-based collision avoidance system, compatible with the aviation industry's current TCAS & ACAS systems, can be implemented for drones, due to the diverse types of drones being used by these tech companies and high cost of TCAS systems. As a result, it is essential the aerial vehicles use transponder-independent collision avoidance systems. The cluster identification and Kalman filter track association algorithms explored in this paper can be easily implemented in drones. Although a low-cost radar system was used to collect data in this paper, the developed algorithms function independent of the type of sensing instrument being used; the sense and track method works as long as the instrument returns position data of local aerial vehicles. Thus, the developed sense and track system can be deployed on a wide array of aerial vehicles, including military aircraft, commercial aircraft, private aircraft, and drones. Furthermore, the transponder-independent solution resolves one of the greatest challenges in implementing a fleet of drones in a real-world setting.

5 Acknowledgments

I would like to thank Aurora Flight Sciences for providing the resources necessary for completing this research project. I would also like to thank my research mentors Jae-Woo Choi, Franklin Wu, and Michael Sardonini for their valuable advice and guidance. I would like to thank my RSI sponsors for enabling this reasearch, and my RSI mentors for providing feedback on my paper. Finally, I would like to thank the Center for Excellence in Education for inviting me to conduct research at MIT and Aurora Flight Sciences as part of the Research Science Institute (RSI) program.

References

[1] A new approach to managing congestion in the skies. *Volpe National Transportation Systems Center*, Apr 2015.

[2] Drone hits passenger plane in canada, Oct 2017.

[3] K. I. Shetty and R. J. Hansman. Current and historical trends in general aviation in the united states. *MIT International Center for Air Transportation (ICAT)*, Aug 2012.

[4] R. Amadeo. Googles waymo invests in lidar technology, cuts costs by 90 percent. *Ars Technica*, Jan 2017.

[5] J. R. Ramsey. The future of air traffic control, Jul 2008.

[6] New better-than-radar technology will boost aircraft tracking. *Tech Bit*.

[7] e. a. Viquerat A. Reactive collision avoidance for unmanned aerial vehicles using doppler radar. *Springer Tracts in Advanced Robotics Field and Service Robotics*, Dec 2007.

[8] e. a. Viquerat A. Reactive collision avoidance for unmanned aerial vehicles using doppler radar, 2008.

[9] L. Blain. Echodyne's amazing miniature uav radar: A huge step towards legal, autonomous drone deliveries, Nov 2016.

[10] Broadband 4g radar specification sheet. *Simrad*.

[11] FAA: ADS-B guidelines. *Federal Aviation Administration*, Feb 2017.

[12] Calculate earth-centered earth-fixed (ecef) position from geodetic latitude longitude and altitude above planetary ellipsoid. *Simulink*.

[13] Convert geodetic latitude and longitude to direction cosine matrix. *Simulink*.